

Article

Mn(II) Sorption on Stream Sediments Sampled in Manganese Mining Area: Dynamics and Mechanisms

Fan Yang, Yankui Tang *, Yuwei Mi, Lu Jiang, Penghong Luo and Yang Yang

School of Resources, Environment and Materials, Guangxi University, Nanning 530004, China; 18776902722@163.com (F.Y.); 18629670151@163.com (Y.M.); kingdomssdabu@163.com (L.J.); penghongLuo@outlook.com (P.L.); Yy123756868505@163.com (Y.Y.)

* Correspondence: cindyktang@gxu.edu.cn; Fax: +86-0771-3273440

Abstract: The stream sediments that have been impacted by manganese (Mn) containing wastewater for decades contain not only abundant microorganisms but also organic/inorganic substances. To achieve effective treatment of manganese (Mn)-containing effluent and recovery of Mn from water/sediments, the Mn(II) sorption behaviors and mechanism on sediments of a stream in Mn mining areas were studied. In addition, the study analyzed the effects of various factors (initial concentration, solution pH, sediment dose, contact time, and coexisting cations) on the Mn sorption efficiency of Daxin sediments, and explored the contribution of microbial activity in the sediment sorption of Mn(II). The results showed that the sorption process of Mn(II) on the sediments was consistent with the Elovich and Freundlich models, and the removal of heavy metals was maximum at 40 °C (62.47–98.93%), pH = 8 (77.51%), initial concentration of 1 mmol·L⁻¹ (95.37%) and sediment dosing of 12 g·L⁻¹ (98.93%). The addition of 50 mM NaN₃ inhibited the microbial activity in the Daxin sediment, reducing the sorption and removal rates of Mn(II) by 0.605 mg·g⁻¹ and 8.92%, respectively. After sorption, the proportion of the Fe–Mn oxidation(iron–manganese) state in Daxin sediments decreased from 54% to 43%, while the proportion of the exchangeable state increased by 10.80%. Microorganisms in the sediment had a positive effect on inhibiting heavy metal migration and reducing the bioavailability of contaminants in the soil. Through this study, we hope to further understand the sorption and desorption mechanism of manganese by stream sediments in manganese ore areas, so as to provide a guide on the management and recovery of Mn from stream sediments in manganese mining areas.

Keywords: manganese mining area; sediment; manganous; sorption



Citation: Yang, F.; Tang, Y.; Mi, Y.; Jiang, L.; Luo, P.; Yang, Y. Mn(II) Sorption on Stream Sediments Sampled in Manganese Mining Area: Dynamics and Mechanisms. *Appl. Sci.* **2022**, *12*, 3368. <https://doi.org/10.3390/app12073368>

Academic Editor: Yosoon Choi

Received: 18 February 2022

Accepted: 24 March 2022

Published: 25 March 2022

Publisher's Note: MDPI stays neutral with regard to jurisdictional claims in published maps and institutional affiliations.



Copyright: © 2022 by the authors. Licensee MDPI, Basel, Switzerland. This article is an open access article distributed under the terms and conditions of the Creative Commons Attribution (CC BY) license (<https://creativecommons.org/licenses/by/4.0/>).

1. Introduction

China, the world's largest producer, consumer, and exporter of electrolytic manganese, plays an important role in global industrial production with an annual production of over one million tons, accounting for more than 97.0% of the global supply [1,2]. However, the development of electrolytic manganese generates a large number of pollutants. Studies have shown that an average of approximately 3 tons of wastewater will be discharged into the environment for every ton of electrolytic manganese produced, while 10–12 tons of electrolytic manganese slag is generated [3,4]. During the leaching of manganese ores, liquid ammonia and ammonium sulphate added during production are required to form NH₄⁺/NH₃ buffer solutions to neutralise the pH for stable electrolytic reduction precipitation of manganese, so the wastewater from electrolytic manganese smelting usually contains Mn and ammonia nitrogen (NH₄⁺-N) [5,6]. Guangxi Zhuang Autonomous Region is one of the most important manganese (Mn) mining areas in China, and the manganese ore resource reserves account for about 23% of the national Mn ore resource reserves [7,8]. Nevertheless, this region is one of the most developed karst regions on earth, with karst areas accounting for about 60% of the total area, therefore, its ecological environment is

extremely fragile and more vulnerable to Mn contamination in surface water as well as groundwater than other regions [9].

Conventional wastewater treatment systems can remove most pollutants, but they do not fully achieve effective removal of large amounts of manganese and ammonia nitrogen, even after standard treatment. Existing processes still have shortcomings such as complexity and high costs, and some processes produce by-products that can even lead to secondary pollution [10]. Constructed wetland (CW) is recognized as the most economical and green technology to intercept such pollutants through plant extraction and microbial stabilization/mineralization. Constructed wetlands use soil, vegetation, and microbial communities to mimic the main structures of natural wetlands. The mechanism of CW treatment of wastewater involves chemical, biological, and physical processes such as sedimentation, filtration, precipitation, volatilization, sorption, plant uptake, and microbial degradation [11–13]. As a carrier for biofilm development in nature, a medium for wetland plant growth, and an adsorbent for pollutant immobilization, river sediments can effectively adsorb heavy metals and other pollutants in the sediment [14]. Microorganisms, especially manganese-oxidizing bacteria, play a crucial role in the purification of metallic Mn and the uptake of $\text{NH}_4^+\text{-N}$. The removal of $\text{NH}_4^+\text{-N}$ depends mainly on the nitrification/denitrification capacity of microorganisms, while the enrichment of inter-rooted microorganisms and ferromanganese oxides contributes to a large extent to the removal of $\text{NH}_4^+\text{-N}$ [15–17]. Therefore, it is essential to explore the effect of sediment as well as microbial activity on manganese sorption in manganese mining areas during the construction of constructed wetlands.

River sediments are complex mixtures of clays, silica, natural organic matter, aluminum, iron and manganese oxides, carbonates, sulfides, certain minerals, and bacteria [18]. As the “sink” of manganese, sediment is not only the final home of manganese but also the place where manganese begins its geochemical cycle. It is worth noting that BMO is one of the most active minerals in terrestrial and aqueous environments, with excellent sorption capacity, large specific surface area and strong oxidizing properties [19]. BMO is capable of immobilizing toxic metals or nutrients from rivers in solid hydroxyl precipitates [20]. As the streams around the mine area have been flowing through the Mn-containing wastewater for a long time, the microorganisms in the sediment have strong sorption and oxidation ability for manganese, and the presence of Mn-oxidizing bacteria (MOB) also contributes to the formation of BMO in the sediment. The continuous production of fresh Mn-oxide provides a large number of new sorption sites for the continuous uptake of manganese. Moreover, the accumulation of proteins in the extracellular polymers (EPS) of microorganisms by the addition of manganese is also an important factor in the extracellular sorption of manganese [21]. Most of the manganese oxides present in soils, sediments and aquatic environments are generally considered to be the result of biological oxidation, and their metabolic processes demonstrate the combined effect of biooxidation and biosorption in manganese purification processes [22].

In the aqueous environment, manganese is often present in the free state (Mn(II)) or insoluble oxidized state (Mn(III) and Mn(IV)) [23]. After being accumulated in the sediment through the sorption process, manganese is utilized as an essential nutrient for the biosystem or oxidized by manganese-oxidizing microorganisms into biological manganese oxide (BMO) [24]. Subsequently, the dissolved Mn(II) was oxidized to Mn(IV) under aerobic conditions, and precipitated to manganese oxides and hydroxides, completing the initial fixation of manganese. Some of the buried manganese oxides and hydroxides in the sediments are reduced to Mn(II) and combined with carbonate in the pore water to form manganese carbonate mineralized deposits in the organic-rich sediment [8]. Since manganese is a transition metal with an alternating redox state, the change of oxygen condition in the sediment easily leads to the reductive dissolution of Mn-oxides [25]. The sorption of Mn(II) by natural sediments is not fully reversible, and the manganese cycle is enhanced with increasing amounts of deposition. Benthic fauna and other physical disturbances allow Mn-containing particles in anoxic subsurface sediments to move to

the oxygenated sediment-water interface, triggering the desorption and oxidation of manganese. Manganese oxide buried below the redox boundary is reduced and dissolved to Mn(II), and Mn(II) diffused upward above the redox boundary is oxidized to insoluble Mn(IV). Subsequently, the generated Mn(II) is adsorbed onto the adjacent manganese oxide or hydroxyl surface. As the manganese reduction process continues, the available sorption sites gradually decrease until saturation is reached. The unadsorbed Mn(II) is then released into the pore water, leading to secondary contamination of the overlying water. The sorption of heavy metal ions by sediments is the key to preventing and controlling the migration of pollutants and plays an important role in the geochemical cycling of heavy metals. To better understand the sorption behaviour of manganese ions in natural systems, we need to further investigate the process and mechanism of manganese sorption/desorption equilibrium for the treatment and effective recovery of manganese metal.

Current studies on sediment sorption of heavy metals have focused on the analysis of the sorption effects of silt, clay, aqueous Fe–Mn oxides and organic matter in them [24]. However, there are fewer studies on the effects of microbial and Fe–Mn oxide transformation processes on heavy metal sorption. For these reasons, the objectives of this study were to (1) Investigate the Mn sorption characteristics of river sediments in the Daxin manganese mining area; (2) Explore the influence of key parameters on the adsorption capacity and Mn sorption efficiency of DX; (3) Develop a thermodynamic and kinetic model for Mn sorption by DX sediments; (4) Discuss the role of microbial activity and Fe–Mn oxides conversion processes in the Mn sorption process.

2. Materials and Methods

2.1. Sampling and Storage

Xialei Manganese Mine (24°54' N, 106°40' E), located in Daxin County, Guangxi Zhuang Autonomous Region, is the largest open-pit manganese mine in China covering an area of 20.46 km². The region has a subtropical monsoon climate with an average annual temperature of 21.3 °C, and an average annual rainfall of 1267.5–1479.2 mm. The experimental soil samples included stream sediments (DX), low-disturbance campus soil (XY) and Luban Lake sediment (LB). DX was collected from a stream in the manganese mining area of Xialei Town, Daxin County, Guangxi, which was basically free of disturbance from agricultural and domestic sewage sources in the upper stream. Due to the long-term high manganese loading of manganese mining streams, the sediments contain high levels of manganese-oxidizing bacteria as well as manganese oxides. To initially investigate the specificity of Mn(II) sorption by stream sediments in the manganese mining area, low-disturbance campus soil (XY) and Lake Luban sediment (LB) within Guangxi University, China, were selected as control groups. XY and LB were both obtained from Guangxi University, China. Soil samples were collected from 0–30 cm of sediment, 80–100 cm of the surface, and around the sampling sites. The samples were thoroughly mixed, then stored in polyethylene boxes sealed at 4 °C.

Pretreatment of the samples before the experiment required the removal of gravels, plant and animal remains, and trash from the collected sediment and soil samples. Subsequently, the samples were placed in a cool and ventilated place to dry naturally. The soil samples were ground to a fine powder, sieved (100 mesh), and sealed for storage.

2.2. Experimental Methods

2.2.1. Comparison of Mn(II) Sorption Properties in Soils

DX, LB and XY were used to compare the sorption performance of manganese from soil samples in different regions. In addition, the pictures of air-dried sediment and sieved sediment are shown in SI (Figure S1). Firstly, the pretreated DX, LB and XY samples were weighed 2.0 g in each conical flask, and 200 mL of MnCl₂ (1 mM Mn(II)) solution was added. To ensure sufficient contact between the soil samples and the Mn-containing solution, the conical flasks were placed in a constant temperature water bath shaker with 180 rpm and

25 °C. During the oscillation process, samples were taken several times at different time intervals to analyze the sorption capacity of different soil samples for Mn(II).

2.2.2. Analysis of Influencing Factors on DX Sorption Performance

To investigate the effects of the initial concentration of the solution, the amount of sediment dosed and the environmental conditions (pH and temperature) on the sorption of Mn(II) by the sediment, a certain amount of DX was weighed mixed with 25 mL of wastewater containing manganese (1 mM Mn(II)), and experiments were conducted using the following ranges of parameters: Solid-to-liquid ratio, 4–12 g·L⁻¹; initial concentration of Mn(II), 1–2 mmol·L⁻¹; initial pH, 5.0–8.0; reaction temperature, 25–40 °C.

The competition of sorption sites in DX is also crucial to the sorption efficiency of Mn(II). Manganese-containing solutions were mixed with solutions containing Cu²⁺, Pb²⁺, Zn²⁺ and Fe²⁺, respectively, to make mixed solutions containing 1 mmol·L⁻¹ Mn(II) with 0.5 mmol·L⁻¹ other metals. After 12 h of sorption reaction, the effect of coexisting cations on the sorption performance of manganese was investigated.

2.2.3. Repeated Sorption

As there were remaining uncontacted sorption sites on the sediment surface after single sorption, it is necessary to repeat the sorption experiment several times to ensure complete saturation of the sorption sites. 0.25 g DX was weighed and placed in a centrifuge tube. Then, the sample was mixed with 25 mL wastewater containing 1 mM Mn(II) and placed horizontally in a constant temperature air bath shaker. After the sorption reaction was carried out for 12 h, the residual manganese concentration was measured. The remaining substrate in the centrifuge tube was placed in a cool and ventilated place to dry. The sorption experiments were repeated until the substrate no longer produced significant Mn(II) sorption, and the remaining substrate was analyzed for the morphology of heavy metal manganese.

2.2.4. Microbial Activity Analysis

To determine the effect of microorganisms on the sediment sorption performance in the manganese mining area, the effect of the microbial inhibitor sodium azide (NaN₃) on the sediment sorption of Mn(II) was analyzed. 0.1–0.3 g DX samples were weighed and mixed with 25 mL of manganese-containing (1 mM Mn(II)) wastewater. Then, 0 mM, 10 mM and 50 mM NaN₃ were added to the well-mixed samples and then placed in a constant temperature water bath shaker for 12 h. The Mn(II) sorption efficiency and changes in chemical forms of heavy metals were analyzed.

2.3. Analytical Methods

2.3.1. Basic Physical and Chemical Properties of Soil

The water content was determined using the drying method. To determine the pH value of the soil, 10 g of the sieved sample was weighed into a 100 mL beaker and 25 mL of distilled water was added with stirring for 1 min to make it homogeneous. After standing for 30 min, the pH was measured using a pH meter. In this study, the international soil texture classification system was chosen to classify soil particles into sand (2000–20 μm), powder (20–2 μm), and clay (<2 μm). Soil organic matter content was determined by the potassium dichromate-sulfuric acid digestion method. The total organic carbon in the soil was oxidized by heating under strong acid conditions using excess K₂Cr₂O₄, and the amount of organic carbon was calculated by using FeSO₄ titration. Soil cation exchange capacity (CEC) was determined using the barium chloride-sulfate forced exchange method. The CEC is determined by measuring the change in sulfuric acid content after the exchange reaction, using the principle that the cations present in the soil can be equivalently exchanged by cations in aqueous barium chloride (BaCl₂). All-element analysis in the sediments was performed using an X-ray fluorescence elemental analyzer (XRF, S8 TIGER, BRUKER, Germany) to determine the composition. Quantification of manganese oxides

in sediments was performed using the Leucoberbelin blue (LBB) standardization method proposed by Matthew in 2019 [26].

2.3.2. Heavy Metal Content and Morphological

The concentrations of heavy metals Mn(II) in the solution were determined by atomic absorption spectrometry (AAS, AA-7000, Shimadzu, Japan), while the concentrations of Pb^{2+} , Zn^{2+} , Cu^{2+} , and Fe^{2+} were determined by plasma emission spectrometry (ICP, ICAP7000, Thermo Fisher, USA). The samples were centrifuged at 5000 rpm for 5 min, and the supernatant was filtered through the 0.45 μ m filter membrane. The samples were acidified with 1% HNO_3 with storage at 4 °C.

Morphological analysis of heavy metals in soils was performed according to the continuous extraction method defined by Tessier in 1979 [27]. A 5-step extraction method was used to detect changes in the morphology and content of five heavy metals fractions (exchangeable, bound to carbonates, bound to iron and manganese oxides, bound to organic matter, residual) in DX sediments before and after sorption of Mn(II).

2.3.3. DNA Extraction and High-Throughput Sequencing Analysis

Macrogenome sequencing was entrusted to Bioengineering (Shanghai) Co., Ltd. for the identification of microbial community and species information in DX sediments. 500 mg of sample was weighed into a centrifuge tube, shaken and mixed with PBS solution. Samples were centrifuged at 10,000 rpm for 3 min at room temperature, and the top layer of liquid was discarded. Centrifuge tubes were inverted on blotting paper for 1 min until no liquid came out. After the treatment, the samples were stored frozen at -80 °C. The E.Z.N.A™ Mag-Bind Soil DNA Kit from OMEGA was used as the extraction kit, and primer 515F (GTGCCAGCMGCCGCGTAA) was used for PCR and fused with a custom V4 primer (GGACTACHVGGGTWTCTAAT) from the sequencing platform.

2.4. Sorption Models

2.4.1. Sorption Kinetic Models

Sorption is a mass transfer process that transfers contaminants from the liquid phase to a solid sorbent. In order to accurately assess information related to heavy metal sorption rates, sediment properties and their mass transfer mechanisms, a kinetic model consistent with the sorption behavior of manganese on DX sediments needs to be determined. In this study, the pseudo-first-order (PFO) kinetic model, the pseudo-second-order (PSO) kinetic model, the Elovich model, and the Webber–Morris model were used to study the kinetic analysis of the interfacial processes. The four kinetic models mentioned above can be represented as follows.

PFO kinetic model:

$$Q_t = Q_e[1 - \exp(-k_1t)] \quad (1)$$

PSO kinetic model:

$$Q_t = \frac{Q_e^2 k_2 t}{1 + Q_e k_2 t} \quad (2)$$

Elovich mode:

$$Q_t = \frac{\ln(a \cdot b)}{b} + \frac{\ln t}{b} \quad (3)$$

Webber–Morris model:

$$Q_t = k_d \cdot t^{\frac{1}{2}} + c \quad (4)$$

where Q_e ($mg \cdot g^{-1}$) is the equilibrium value of adsorbed Mn(II), t (min) is the sorption time (min), k_1 (min^{-1}) and k_2 ($g \cdot mg^{-1}$) are the pseudo primary and pseudo secondary rate constants, respectively. In the Elovich equation, a ($mg \cdot (g \cdot min)^{-1}$) is the constant on the initial sorption rate, b constant is the surface coverage and chemical Intraparticle diffusion equation, k_d ($mg \cdot (g \cdot min^{1/2})^{-1}$) is the rate constant for intraparticle diffusion, c is the intercept of the y -axis [28].

2.4.2. Sorption Thermodynamic Models

The sorption isotherm, which describes the mechanism of adsorbent-adsorbent interaction, is essential to optimize the use of adsorbents. The Langmuir isotherm model is often used under the assumption of a fixed number of homogeneous positions, where reversible monolayer sorption occurs in the absence of interaction between adsorbent species. It can be expressed by the following equation:

$$Q_e = \frac{Q_{max}K_L C_e}{1 + K_L C_e} \quad (5)$$

where Q_{max} ($\text{mg}\cdot\text{g}^{-1}$) is the maximum saturated monolayer sorption capacity, K_L ($\text{L}\cdot\text{mg}^{-1}$) is the Langmuir sorption equilibrium constant related to the affinity between the adsorbent and the adsorbent, and C_e is the equilibrium concentration of Mn(II) in solution ($\text{mg}\cdot\text{L}^{-1}$) [29].

The Freundlich model primarily describes multilayer sorption of surface inhomogeneous adsorbents which applies to the sorption of solutes in solution on solid surfaces. The model describes reversible, non-ideal, multilayer sorption, and is commonly used for non-homogeneous adsorbents such as biomass. It is expressed as follows:

$$Q_e = K_F C_e^{\frac{1}{n}} \quad (6)$$

where Q_e ($\text{g}\cdot\text{kg}^{-1}$) is the amount of metal adsorbed by the sediment at equilibrium, C_e ($\text{g}\cdot\text{kg}^{-1}$) is the equilibrium concentration, K_F ($\text{g}\cdot\text{kg}^{-1}$) is the Freundlich isotherm constant, and n is the dimensionless constant indicating the heterogeneity factor [30].

2.5. Statistical Analysis

All experimental measurements were made in triplicate, and all experiments were repeated at least twice. The mean and standard deviation were evaluated by one-way analysis of variance (ANOVA). The experimental data were treated statistically using EXCEL software. Correlation coefficients were fitted using the software Origin Pro 2018 to determine the kinetic and isotherm models suitable for the sorption of Mn(II) from DX sediments.

3. Results and Discussions

3.1. Analysis of Physicochemical Properties in DX Sediments

The results of water quality and sediment physicochemical properties of the streams at the sampling sites are shown in Tables 1 and 2. The pH of the stream at the sampling site was 7.3, showing weak alkalinity. Due to the long-term flow of the stream through the manganese mining and smelting wastewater, the concentration of Mn(II) ($3.85 \text{ mg}\cdot\text{L}^{-1}$) and ammonia nitrogen ($14.3 \text{ mg}\cdot\text{L}^{-1}$) in the water was high. The equivalent concentration of Mn (IV) in the sediment was calculated to be approximately 6.66% based on the LBB standardization method. The evidence demonstrated that the sorption capacity of manganese oxide is an important factor in the efficiency of manganese purification, and can be used to examine the potential for using this sediment to recover manganese in the construction of CW. In addition, SiO_2 (48.4%) were the main component of the sediment. The heavy metal cation exchange capacity (CEC) was $14.21 \text{ cmol}\cdot\text{kg}^{-1}$, indicating a high negative colloidal charge, which contributes to the electrostatic sorption of Mn(II). As a key substance to promote the sorption of heavy metals, iron and manganese oxides account for more than 10% of the total weight of the solid phase.

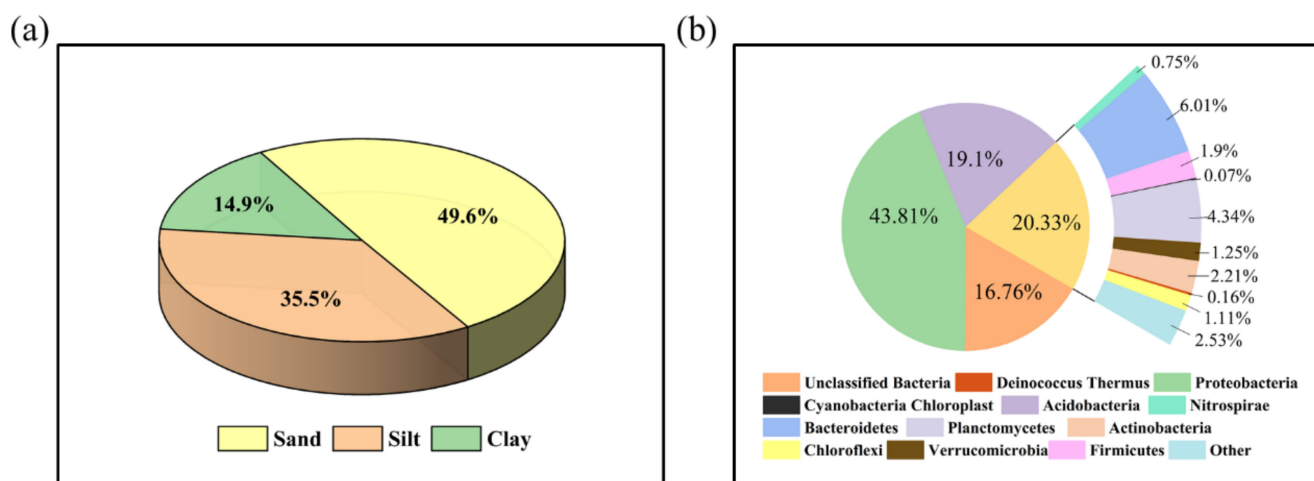
Table 1. Basic water quality of streams at sampling sites in manganese mining areas.

Temperature (°C)	pH	DO (mg·L ⁻¹)	Conductivity (µs)	Turbidity (NTU)	NH ₄ ⁺ (mg·L ⁻¹)	TP (mg·L ⁻¹)	Mn(II) (mg·L ⁻¹)
22.6	7.3	6.6	832	2.61	14.3	0.05	3.85

Table 2. Basic physicochemical properties of sediments in the manganese mining areas.

Organic Matter (g/kg)	pH	CEC (cmol·kg ⁻¹)	Moisture Content (%)	SiO ₂ (%)	Al ₂ O ₃ (%)	CaO (%)	MnO (%)	Fe ₂ O ₃ (%)
28.5	7.62	14.21	46.38	48.4	6.38	6.08	5.28	4.86

Figure 1 reflects the textural classification and microbial community composition of the soils in the DX sediments. Soil texture was dominated by sand (49.6%) and meal (35.5%) grains. The percentage of clay particles in DX sediments is 14.9%, which is higher than the content of clay particles in many regions. As the main site of negative charge concentration in the soil, clay particles can form complex colloids with humus. The study showed that soils containing higher clay particles have a greater capacity for Mn(II) sorption.

**Figure 1.** Analysis of Daxin sediment properties. Soil texture classification (a); microbial community composition (b).

MOB, with a strong sorption capacity for Mn(II), are widely found in environments containing large amounts of manganese as well as an active manganese cycle. The EPS secreted by MOB can also promote the sorption of Mn(II) [31]. In DX sediments, the relative abundance of Proteobacteria and Acidic Bacteria was 43.81% and 19.10%, respectively, and were the dominant microorganisms in the soils of the sampling area, which have been shown to be MOB. The research shows that the isolated MOB is mainly concentrated in the Firmicutes, Actinobacteria, Bacteroidetes, Proteobacteria and Acidobacteria [32]. In addition, the colony structure at the sediment genus level is shown in SI Table S1. Many genera with strong manganese oxidation properties were present in DX sediments, such as *Acinetobacter*, *Pseudomonas*, *Rhizobium*, *Sphingomonas*, *Exiguobacterium*, *Pseudoxanthomonas* genera.

3.2. Effect of Operating Variables

3.2.1. Sorption Performance and Equilibrium Time

The effect of contact time on the sorption of Mn(II) by DX, LB, and XY samples is shown in Figure 2. The sorption capacities of Mn(II) varied greatly among samples, and the final sorption effect of each experimental group was DX (4.42 mg·g⁻¹) > LB (2.99 mg·g⁻¹) > XY (0.63 mg·g⁻¹). The final Mn(II) removal rate of DX was as high as 84.85%, and its

sorption performance was much higher than that of LB and XY. In particular, the DX river sediment was loaded with manganese for a long time, and the abundance of Mn-containing microorganisms and Fe–Mn oxides were both at a high level. In addition, the sorption of heavy metal Mn(II) showed a similar trend for each soil sample. During the transient sorption stage (0–60 min), the adsorbent provided more adsorbable sites, and the sorption reaction could occur freely [33]. The contribution of this stage to the sorption of heavy metals Mn(II) was more significant, and more than 90% of manganese was adsorbed. In particular, the sorption rates of DX, LB and XY in the first 5 min of the sorption process were as high as 56.96%, 35.86% and 12.24%, respectively. Next, the gradual sorption phase (60–420 min) controlled the Mn(II) sorption rate by intra-particle diffusion in the soil particles. As the sorption reaction continues, the sorption rate decreases until the sorption sites are filled with Mn(II), finally reaching equilibrium after 720 min. During the diffusion of free Mn(II) from the surface to the interior of soil particles, complex precipitates are continuously formed on the surface and inside the soil particles, which is also an important reason for the decrease in Mn(II) concentration [34]. Preliminary results showed that DX was specific for Mn(II) sorption, so the DX was used in the subsequent experiments, and the sorption time was set to 12 h to ensure the sorption equilibrium.

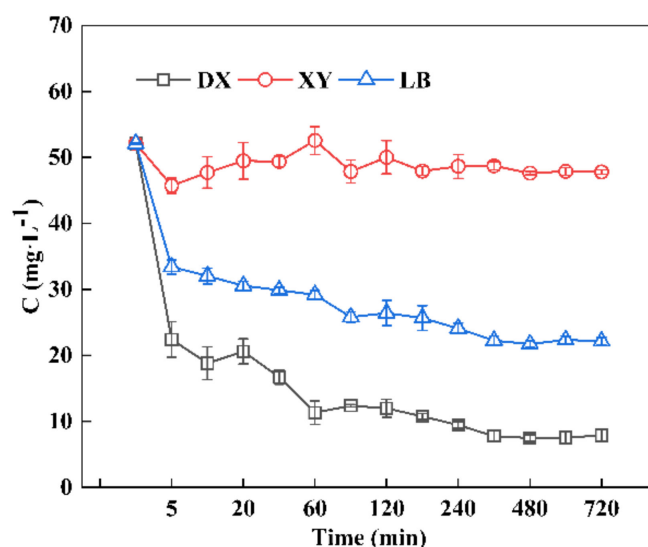


Figure 2. Sorption effect of manganese on three different soil samples.

3.2.2. Effect of Initial Manganese Concentration in Solution on Mn(II) Sorption

To investigate the applicable characteristics of DX adsorbent, the effect of initial concentration in the solution on Mn(II) sorption was studied (Figure 3). With the increase in the initial concentration of Mn(II) in the solution, the sorption of DX increased, but the removal of Mn(II) decreased significantly. When the initial DX dosage was $12 \text{ g}\cdot\text{L}^{-1}$, the sorption amount of DX on Mn(II) was $4.70 \text{ mg}\cdot\text{g}^{-1}$ in the solution with the initial concentration of Mn(II) of $1 \text{ mM}\cdot\text{L}^{-1}$, and the removal rate was as high as 95.37%. The sorption of DX was enhanced by 15–30% at the initial concentration of $1.5 \text{ mM}\cdot\text{L}^{-1}$ versus $2.0 \text{ mM}\cdot\text{L}^{-1}$, but its removal rate of Mn(II) was reduced by 12–32%. The initial metal ion concentration provides the necessary driving force to overcome the metal mass transfer resistance between the water-solid phase and is an important factor affecting the heavy metal sorption efficiency. Although low metal ion concentrations provide lower driving forces, the number of ions competing for available active sites in the biomass is also low. Sufficient surface area exists to absorb the available ions in the liquid phase, so the sorption capacity of DX is limited, while the removal of Mn(II) is at a high level [35]. As the initial metal concentration increases, the driving force of the active biosorption sites increases, resulting in an enhanced equilibrium sorption capacity of the DX adsorbent [36]. However, the saturation of available biosorption sites on the biosorbent surface prevented further binding of metal ions,

which led to significant inhibition of manganese ion removal. Therefore, the availability and sorption capacity of active biosorption sites on the surface of biosorbents are key factors affecting effective metal uptake efficiency. In practical applications, suitable adsorbents should be selected according to the heavy metal concentration of the wastewater.

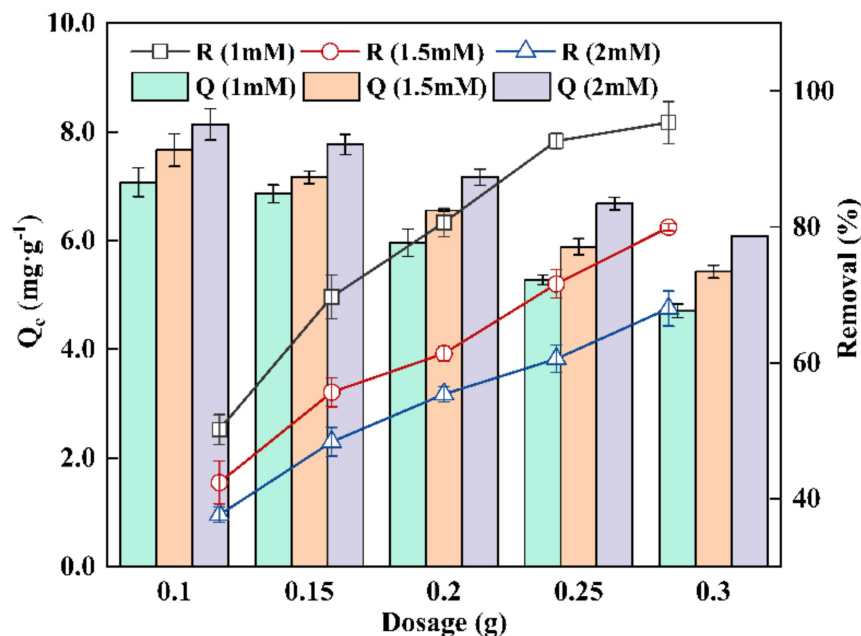


Figure 3. Effect of initial concentration of solution on the sorption effect of manganese.

3.2.3. Effect of Temperature and Sediment Solid-Liquid Ratio on Mn(II) Sorption

Temperature is an important factor affecting the stability constants of heavy metal conditions. Figure 4 show the sorption capacity and removal rate of DX on heavy metal Mn(II) at different temperature conditions (25 °C, 30 °C and 40 °C). The results show that the increase of temperature is favorable to promote the sorption of heavy metal Mn(II) by sediment DX. Both the sorption amount and removal rate of Mn(II) reached the maximum at the reaction temperature of 40 °C. When the initial dosage was $\text{g}\cdot\text{L}^{-1}$, the sorption and removal rates of Mn(II) at 25 °C were $7.07 \text{ mg}\cdot\text{g}^{-1}$ and 50.16%, respectively, while they were increased by 1.30 and 1.26 times at 40 °C. Temperature affects the sorption process in two main ways. From the kinetic point of view, the increase in temperature contributes to the decrease in solution viscosity, which accelerates the diffusion rate of adsorbent molecules through the external boundary layer and the internal pores of the adsorbent particles. On the other hand, the enhancement in sorption capacity of the adsorbent with increasing temperature is facilitated by the rise in Mn(II) mobility, which makes the diffusing ions less hindered [37]. Changes in soil properties (pore size and carbon activity) by elevated temperature may also be important in promoting heavy metal sorption capacity and efficiency [38].

The amount of sediment dosing directly determined the number of total sorption sites and the amount of cation exchange in the solution. The effect of sediment solid-liquid ratio was adjusted to $4\text{--}12 \text{ g}\cdot\text{L}^{-1}$ by varying the DX dosage, and its effect on the sorption of Mn(II) was investigated (Figure 4). With the increase of sediment dosage, the removal of Mn(II) increased significantly from 50.16–62.47% to 95.37–98.93%. However, the sorption of Mn(II) basically reached saturation when the sediment dosage was $10 \text{ g}\cdot\text{L}^{-1}$. The removal rate of Mn(II) from the solution by DX was more than 95%, and almost no longer changed significantly with the increase of the solid-liquid ratio. Nevertheless, the sorption of Mn(II) showed a linear decrease with an increasing solid-liquid ratio. At 25 °C, the sorption of Mn(II) decreased from $7.07 \text{ mg}\cdot\text{g}^{-1}$ to $4.70 \text{ mg}\cdot\text{g}^{-1}$ by the increasing solid-liquid ratio. The elevated adsorbent concentration contributes to the increase of surface-active exchange

sorption sites with total surface cation exchange, which promotes the sorption of DX on Mn(II). Due to the interference caused by the interaction between the active sites of the adsorbents, the solute sorption per unit weight of adsorbent decreases with increasing adsorbent concentration [39]. It is noteworthy that the increase in solid-liquid ratio did not significantly improve the removal rate when Mn(II) was largely removed from the solution, but the sorption amount continued to decrease. When the sediment dosing was increased from $10 \text{ g}\cdot\text{L}^{-1}$ to $12 \text{ g}\cdot\text{L}^{-1}$ at 40°C , the removal rate basically did not change significantly, but the sorption amount decreased significantly from $5.74 \text{ mg}\cdot\text{g}^{-1}$ to $4.87 \text{ mg}\cdot\text{g}^{-1}$, which is consistent with the results of Amer and Nowruzi et al. [40,41].

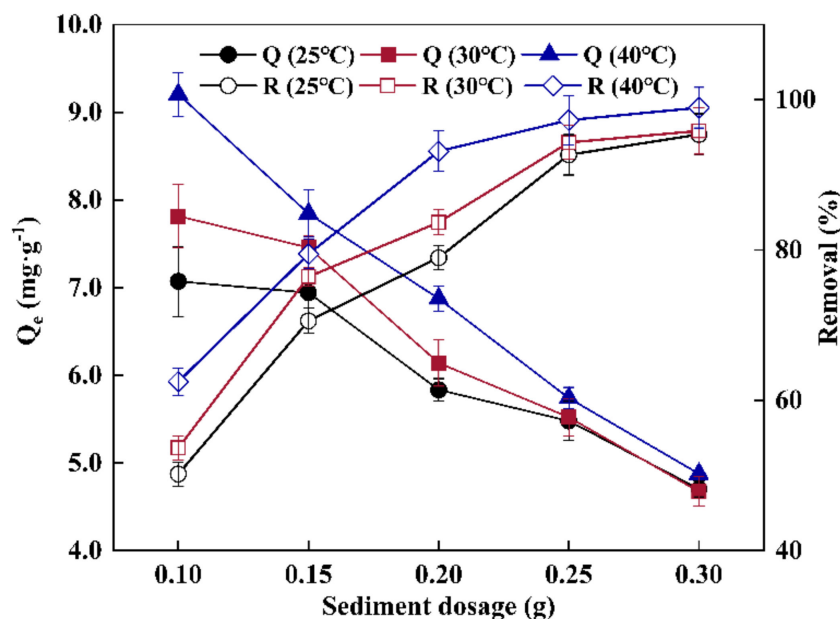


Figure 4. Effect of different temperatures on the sorption effect of manganese.

3.2.4. Effect of pH on Mn(II) Sorption

The pH value affects the surface characteristics of soil particles and the fugitive form of heavy metals and has a strong influence on the sorption of the Mn(II) [42]. The effect of pH on the sorption capacity of DX manganese is shown in Figure 5. With the increase of pH from 5 to 8, the sorption and removal of Mn^{2+} achieved an increase of $0.50 \text{ mg}\cdot\text{g}^{-1}$ and 9.97%, respectively, and finally up to $5.73 \text{ mg}\cdot\text{g}^{-1}$ and 77.51%. At pH 6–8, DX could achieve more than 70% of Mn^{2+} sorption efficiency. Ion exchange is the main metal sorption mechanism in the solution. At low pH, most of the sorption sites were bound to H^+ , which had a competitive sorption relationship with Mn(II). With the increase of pH, the decrease of H^+ makes the competitive relationship weaker, resulting in the significant improvement of Mn(II) sorption capacity and sorption efficiency. Meanwhile, the effect of pH on the surface potential of the sediment was also an important reason for the improvement of the sorption capacity. As the pH increases, the negative charge companions on the surface of clay minerals and soil organic matter in the soil increase, which facilitates the sorption of DX on manganese ions in the solution [43].

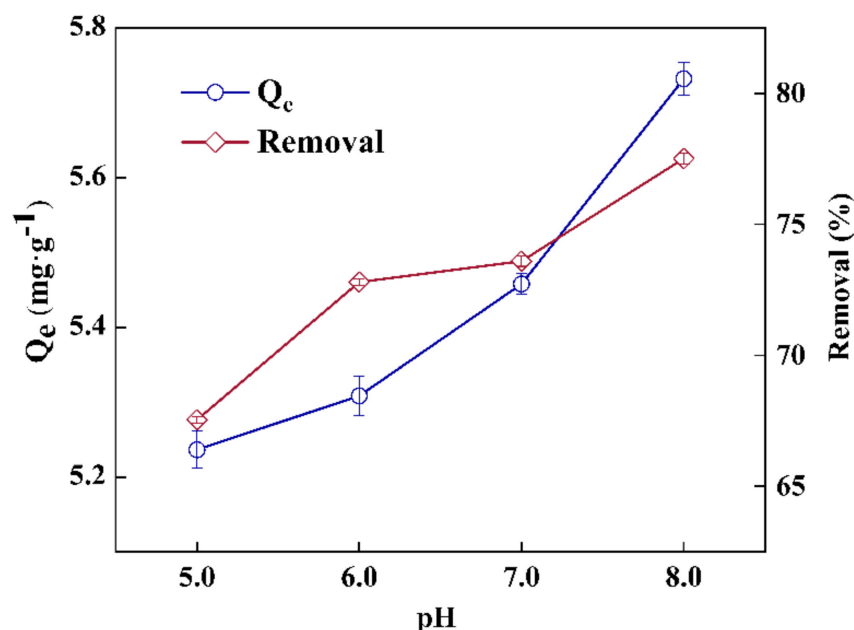


Figure 5. Effect of pH on the sorption effect of manganese.

3.2.5. Effect of Coexisting Cations on Mn(II) Sorption

Industrial wastewater is usually a complex system of multiple ions, and the cations present in the solution will compete with the heavy metal ions to be removed for sorption sites, thus affecting the sorption capacity of the adsorbent for heavy metal ions. The effect of coexisting cations on the sorption of manganese by DX is shown in Figure 6. Without the addition of other metal ions, the sorption and removal rates of Mn(II) by DX were better, as high as $5.38 \text{ mg}\cdot\text{g}^{-1}$ and 90.22%, respectively. The addition of other metal ions (Pb^{2+} , Zn^{2+} , Cu^{2+} and Fe^{2+}) had an inhibitory effect on the sorption of Mn(II). In particular, the inhibitory effect of Zn^{2+} was the most obvious, resulting in a decrease of $2.01 \text{ mg}\cdot\text{g}^{-1}$ and 29.97% in the removal and sorption of Mn(II). The inhibition effect of Pb^{2+} , Fe^{2+} , Cu^{2+} metal ions on Mn(II) sorption was similar, and the removal efficiency was reduced by 18.30–22.37%. The phenomenon resulted from the easy formation of covalent bonds with the sorption sites during Zn^{2+} sorption, which formed a strong competition with Mn(II). Meanwhile, DX showed a purification effect for all heavy metals in aqueous solution, with sorption amounts of Pb^{2+} ($9.01 \text{ mg}\cdot\text{g}^{-1}$) > Cu^{2+} ($2.89 \text{ mg}\cdot\text{g}^{-1}$) > Zn^{2+} ($2.15 \text{ mg}\cdot\text{g}^{-1}$) > Fe^{2+} ($1.51 \text{ mg}\cdot\text{g}^{-1}$) in that order. The competitive sorption of heavy metal ions in the soil was significantly correlated with the electronegativity of the ions, the primary hydrolysis coefficient, the ratio of charge to the radius, and the magnitude of the Misono softness coefficient [44]. The adsorption process of heavy metal ions is dominated by physical adsorption, chemisorption and ion exchange. Compared with the single Mn(II) system, metal ions competing with Mn(II) for adsorption sites exist in the mixed cationic composite solution, thus affecting the adsorption efficiency of Mn(II). Therefore, exploring the adsorption-desorption process of the actual wastewater from the manganese mining area still needs to be explored in-depth with the actual wastewater composition.

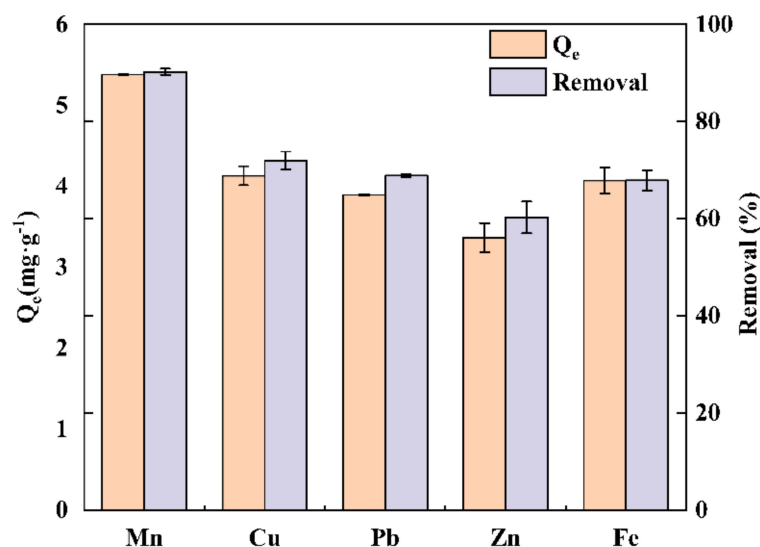


Figure 6. Effect of coexisting cations on manganese sorption.

3.2.6. Repeated Sorption

The sediment DX surface usually had remaining uncontacted sorption sites after one sorption. In order to achieve full sorption of heavy metal Mn(II) by DX, the sediments that had reached the sorption equilibrium state was air-dried and then adsorbed several times (Figure 7). When the DX sorption sites were not completely occupied, the DX still had some sorption capacity for Mn(II) during multiple repetitions of sorption, with significant decreases in both sorption amount and removal rate. The initial sorption and removal rates of Mn(II) were 5.11 mg·g⁻¹ and 90.59%, respectively, which decreased to 2.31 mg·g⁻¹ and 43.62% at the second sorption. After five repeated sorptions, the DX sediments basically reached the sorption saturation state with the removal rate finally only 2.85%. Since the already adsorbed Mn(II) is partially oxidized, there are remaining binding sites in the adsorbent, so a more appreciable removal rate can still be observed by repeating the sorption process. In addition, the generated MnO_x can also provide more sorption sites for the removal of Mn(II). However, the heavy metal removal efficiency decreases with a further increase of MnO_x content. It indicates that there is a specific threshold of sorption sites within which the mixed adsorbent can exhibit the maximum sorption efficiency. Overcrowding of MnO_x particles on the clay surface may also lead to overlapping sorption [45].

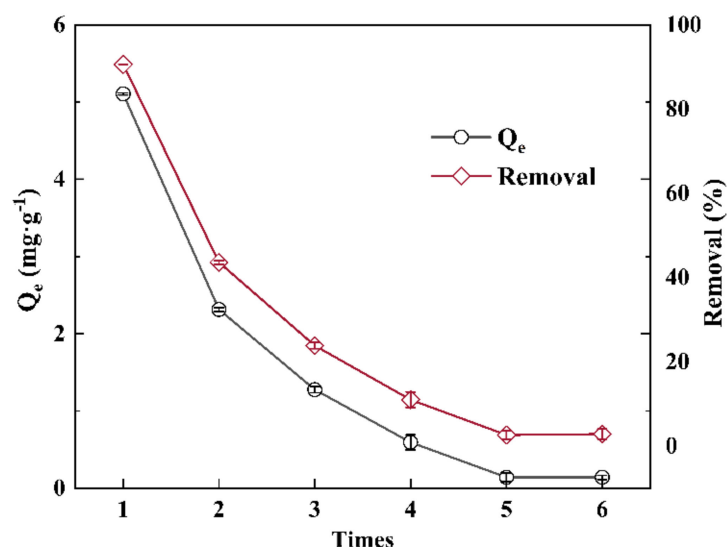


Figure 7. Repeated sorption using DX after sorption equilibrium state several times.

3.3. Exploring the Mechanism of Manganese Sorption Using DX

3.3.1. Sorption Kinetic Model

To determine the process and mechanism of Mn(II) sorption by DX samples, the kinetic models were determined using the pseudo-first-order, pseudo-second-order, internal particle diffusion and Elovich models (Figure 8). The parameters and regression coefficients (R^2) of the kinetic model for Mn(II) sorption in soils are shown in Table 3. The results showed that the PFO and internal diffusion models were poorly fitted, with R^2 only 0.886 and 0.570, respectively. Compared with the PSO model (0.952), the Elovich model with an R^2 of 0.994 can better simulate the sorption of Mn(II) by DX. It is demonstrated that the sorption process is mainly chemisorption, and the efficiency of the sorption process is influenced by both the adsorbent and the adsorbent mass. In addition, soils have continuous sorption sites during sorption, and the Elovich model is applicable to this type of sorption process with large variations in activation energy, which increases linearly with surface coverage [46]. The Elovich equation has been applied in many sorption systems containing metals (Pb^{2+} , Cr^{3+} , Cr^{6+} , Cd^{2+} , Cu^{2+} , Se^{4+} , As^{5+} , K^+ , Pb^{2+} , etc.). Largitte simulated the kinetics of lead sorption on activated carbon using 10 kinetic models, with the results confirming that the simplified Elovich and Elovich simulated the data better [47]. Therefore, the Elovich model is the most consistent kinetic model for Mn(II) sorption on DX. In practical engineering applications, it is important to determine the effective sorption operation time applicable to the sorption system described by the Elovich equation.

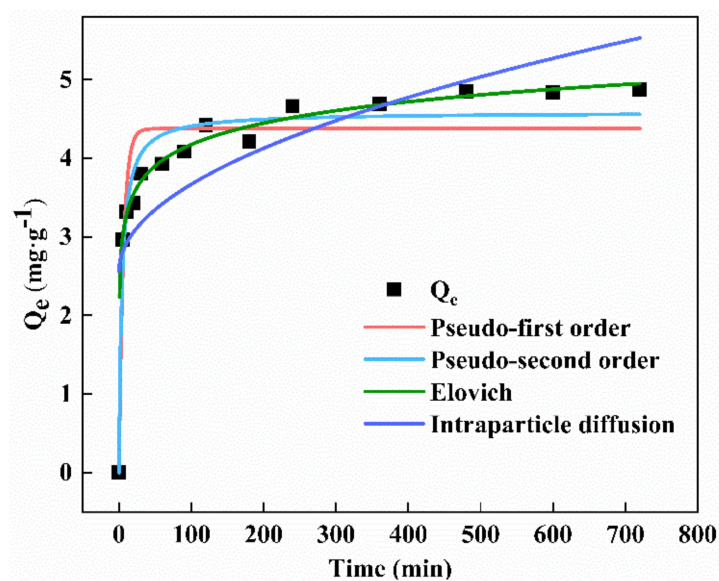


Figure 8. Kinetic equation fitting curve for manganese sorption.

Table 3. Parameters and regression coefficients of the sorption kinetic model.

Model	Parameter	R^2
Pseudo-first-order	$k_1 = 0.165$	0.886
Pseudo-second-order	$k_2 = 0.055$	0.952
Elovich	$a = 162.099; b = 2.545$	0.994
Intraparticle diffusio	$k_d = 4.584; c = 0.055$	0.570

3.3.2. Isothermal Sorption Model

The sorption experimental data in this study were described using the Langmuir and Freundlich model sorption isotherms (Figure 9). The calculated constant parameters and correlation coefficients for each isotherm model are shown in Table 4. The R^2 for the Langmuir models were 0.917 and 0.938 at 25 °C and 40 °C, but only 0.875 at 30 °C. Therefore, the Langmuir model can only be used to describe the sorption of Mn(II) in

DX under certain temperature conditions. The R^2 of the Freundlich models were all greater than 0.936, indicating that the model is applicable to describe the sorption process at all temperature conditions, proving that the sorption process is a multilayer sorption system [48,49]. Meanwhile, the adsorbent sorption strength (n) was much greater than 1 at all temperatures, explaining the easy sorption characteristics of DX for Mn(II).

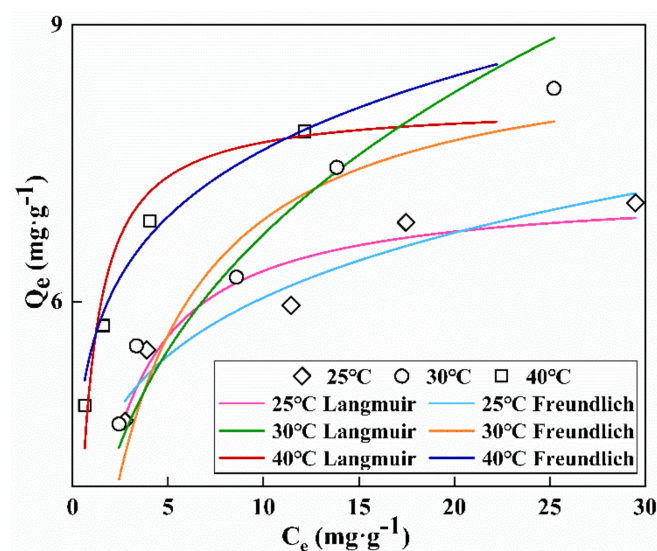


Figure 9. Thermodynamic fitting curve of adsorbed manganese.

Table 4. Parameters and regression coefficients of the sorption thermodynamic model.

Temperature	Langmuir			Freundlich		
	K_L $L \cdot mg^{-1}$	Q_{max} $mg \cdot g^{-1}$	R^2	K_F $g \cdot kg^{-1}$	n	R^2
25 °C	0.693	7.245	0.917	4.193	6.291	0.936
30 °C	0.350	8.851	0.875	3.392	3.362	0.972
40 °C	1.868	8.140	0.938	5.492	6.966	0.984

3.4. Effect of NaN_3 on Microbial Activity

Microbial communities play a key role in the biogeochemical cycle of pollutants, influencing the fate of pollutants through degradation, sorption, and redox [50]. Microbial sorption is considered an important process for removing heavy metals from the environment. NaN_3 is a strong metabolic inhibitor of the respiratory chain, which inhibits microbial growth and unique microbial activities [51]. To investigate the role of microbial communities in sediment sorption, the effects of different concentrations of NaN_3 on the sorption capacity and Mn(II) sorption efficiency of DX were analyzed (Figure 10). The results showed that the sorption capacity of DX sediments and its Mn(II) removal efficiency was reduced by NaN_3 . When DX was dosed at $10 g \cdot L^{-1}$, the sorption and removal rate of DX with 50 mM NaN_3 decreased by $0.605 mg \cdot g^{-1}$ and 8.92%, respectively, compared with no NaN_3 addition. The process of biogeochemical cycling of Mn(II) in soils is very complex and redox reactions involving Mn(II) are influenced by various physical, chemical, and microbial processes. Under natural nutrient conditions, 50 mM NaN_3 severely inhibits microbial activity, resulting in a significant reduction in extracellular proteins and enzymes secreted by bacteria, making the efficiency of Mn(II) sorption and oxidation significantly lower [51]. Iram and Abdu also found the biosorption properties of soil microorganisms for heavy metal ions, and soil microorganisms can be used directly for remediation of contaminated soils [52,53]. In addition, the alteration of microbial activity also affects soil pH, redox status, heavy metal solubility and bio-enzymes.

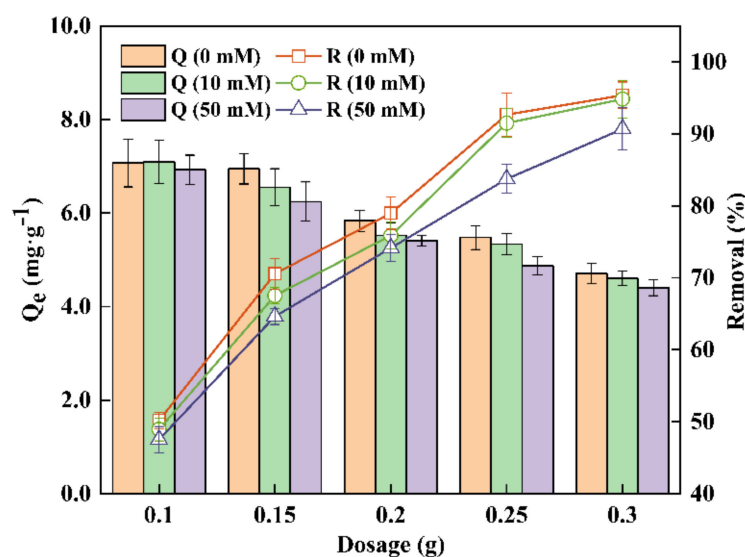


Figure 10. Effect of adding sodium azide to inhibit microbial action on manganese sorption.

3.5. Analysis of Changes in Chemical Forms for Heavy Metals

Figure 11 shows the changes in the chemical morphology of manganese before and after sorption of DX under different conditions. In the original sample of DX, the contents were ranked as Fe–Mn bound state ($5.41 \text{ mg}\cdot\text{g}^{-1}$) > residual state ($0.69 \text{ mg}\cdot\text{g}^{-1}$) > exchangeable state ($0.50 \text{ mg}\cdot\text{g}^{-1}$) > organic matter bound state ($0.24 \text{ mg}\cdot\text{g}^{-1}$) > carbonate bound state ($0.13 \text{ mg}\cdot\text{g}^{-1}$). The Fe–Mn oxide bound state accounts for more than 70% of the total manganese mass in DX and is the part of Fe_2O_3 and MnO_2 , etc. that generates soil nodules in a relatively stable form. The exchangeable state is the part that changes more before and after sorption, which generally refers to heavy metals exchanged and adsorbed on soil clay minerals and other components, such as iron hydroxide, manganese hydroxide and humus. It is the most sensitive to changes in the soil environment and is most readily absorbed by crops. Moreover, heavy metals in the residual (8–10%) are stably present in the lattice of quartz and clay minerals, etc., which have little effect on soil heavy metal migration and bioavailability. Both the carbonate-bound state and the organic matter-bound state accounted for less than 4%, and hardly changed significantly before and after sorption. The carbonate-bound state is sensitive to soil environmental conditions. As the soil pH decreases, a large amount of released ionic state heavy metals are taken up by the crop. The organic matter bound state is the one that enters the organic matter in different forms and then undergoes chelation to form chelated salts or sulfides. In general, this form is not easily absorbed and used by organisms.

The change in the percentage of manganese morphology after sorption, net of DX background values, is shown in Figure 12. During the sorption of Mn(II) by DX sediments, both the residual state and the organic matter-bound state accounted for a relatively low proportion of the total heavy metal chemistry and did not change significantly. Compared to single sorption, the proportion of exchangeable state gradually decreased from 38% to 29% after reusing DX sediments sorption, but the proportion of Fe–Mn oxidation state increased by 4%. The reason for this phenomenon is the oxidation of a part of previously adsorbed Mn(II) by the action of microorganisms to form manganese oxides, which combine with new heavy metal ions to generate soil nodules. The hydroxide of Mn(II) combined with CO_2 in the air to generate new carbonate groups, resulted in a rise of about 6% in the carbonate-bound state after repeated sorption. In addition, the percentage of the Fe–Mn oxidation state and the exchangeable state changed significantly after the addition of NaN_3 . With the increase of NaN_3 concentration, the proportion of Fe–Mn oxidation state decreased, while the proportion of exchangeable state increased. When 50 mM NaN_3 was added, the proportion of the Fe–Mn oxidation state decreased from 54% to 43%, and the exchangeable state increased by 10.80%. This evidence proves that the inhibitory

effect of NaN_3 on microorganisms is the main reason for the decrease of Mn(II) sorption efficiency. Microorganisms play a key role in heavy metal sorption, especially in Fe–Mn oxide generation. Under the action of microorganisms, the easily released Mn(II) in the exchangeable and carbonate-bound states in the sediment can gradually form a relatively stable Fe–Mn-bound state, thus stabilizing mineralization in a long-term natural cycle. Therefore, microorganisms in sediments have a positive impact on inhibiting the migration of heavy metals in soils.

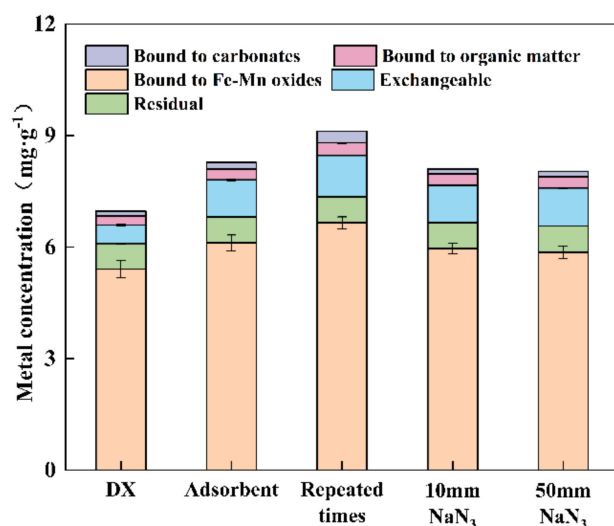


Figure 11. Chemical morphology analysis of manganese before and after sorption. where “Adsorbent” refers to a sample after a single sorption, and “Repeated times” refers to a sample after six repetitions.

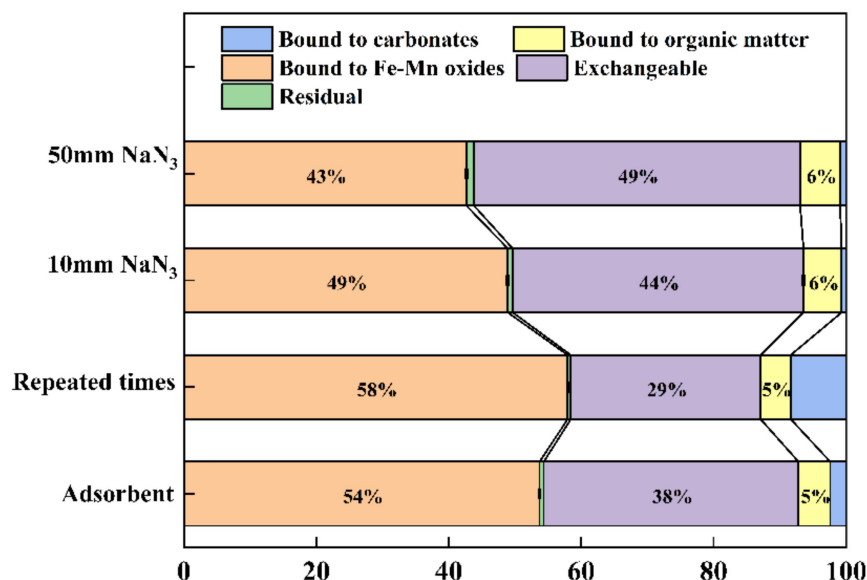


Figure 12. Proportion of each chemical form of adsorbed manganese after deducting background values.

4. Conclusions and Perspectives

In this study, we evaluated the sorption effect of sediment DX on Mn(II) in the Daxin manganese mining area and explored the importance of microorganisms on heavy metal sorption. It is confirmed that microorganisms abundant in natural sediments and iron and manganese oxides play a key role in the removal of Mn(II) . Due to the uncertainty and continuous dynamic changes of natural systems, the process of heavy metal sorption by soils is extremely complex. In this study, the dynamic process of heavy metal sorption

was investigated, providing a scientific basis for the in-situ remediation of heavy metal pollution. The main results obtained in this study are as follows.

- (1) The sorption capacity of Mn(II) differs greatly among different soil sample types. When the sediment dosage was $10 \text{ g}\cdot\text{L}^{-1}$, DX has a good effect on Mn(II) removal and the final removal rate up to 84.85%. Its sorption performance was much higher than that of LB and XY.
- (2) The sorption process follows the Elovich model ($R^2 = 0.994$) and Freundlich model ($R^2 = 0.936\text{--}0.984$). The sorption process is mainly based on multi-molecular layer chemisorption, which is jointly influenced by the adsorbent and adsorbent mass.
- (3) Environmental factors had a significant effect on the Mn(II) sorption process. In a certain range, the increase of temperature, sediment dosage ($4\text{--}12 \text{ g}\cdot\text{L}^{-1}$) and pH were favorable to promote the sorption of Mn(II) by the sediment DX.
- (4) After five repetitions of sorption, the sorption sites of DX reached basic saturation when the sediment dosage was $10 \text{ g}\cdot\text{L}^{-1}$. Meanwhile, in mixed heavy metal solutions, the presence of Pb^{2+} , Zn^{2+} , Cu^{2+} and Fe^{2+} coexisting cations all inhibited the sorption of Mn(II), especially Zn^{2+} .
- (5) Microorganisms played a key role in the process of heavy metal sorption and Fe–Mn oxide generation. The addition of NaN_3 inhibited the activity of microorganisms in the soil, and the content of exchangeable and carbonate-bound manganese increased, while the content of Fe–Mn bound state decreased.

Supplementary Materials: The following supporting information can be downloaded at: <https://www.mdpi.com/article/10.3390/app12073368/s1>, Figure S1: Air-dried sediment and sieved sediment, Table S1: Relative abundance of 16S rRNA gene sequences classified to genus levels.

Author Contributions: Conceptualization, F.Y. and Y.T.; methodology, F.Y.; software, P.L.; validation, L.J., Y.Y. and F.Y.; formal analysis, F.Y.; investigation, F.Y.; data curation, F.Y.; writing—original draft preparation, F.Y.; writing—review and editing, Y.M. and Y.T. All authors have read and agreed to the published version of the manuscript.

Funding: This study was financially supported by the National Natural Science Foundation of China (No. 51668006); the Foundation of Guangxi Key Laboratory of Clean Pulp & Papermaking and Pollution Control, College of Light Industry and Food Engineering, Guangxi University (No. 2019KF29); the Innovation Project of Guangxi Graduate Education (No. YCSW2021015 and No. YCBZ2021016).

Institutional Review Board Statement: Not applicable.

Informed Consent Statement: Not applicable.

Data Availability Statement: Not applicable.

Conflicts of Interest: The authors declare no conflict of interest.

References

1. Duan, N.; Dan, Z.; Wang, F.; Pan, C.; Zhou, C.; Jiang, L. Electrolytic manganese metal industry experience based China's new model for cleaner production promotion. *J. Clean. Prod.* **2011**, *19*, 2082–2087. [[CrossRef](#)]
2. Xu, F.; Jiang, L.; Dan, Z.; Gao, X.; Duan, N.; Han, G.; Zhu, H. Water balance analysis and wastewater recycling investigation in electrolytic manganese industry of China—A case study. *Hydrometallurgy* **2014**, *149*, 12–22. [[CrossRef](#)]
3. Zhang, Y.; Liu, X.; Xu, Y.; Tang, B.; Wang, Y.; Mukiza, E. Preparation and characterization of cement treated road base material utilizing electrolytic manganese residue. *J. Clean. Prod.* **2019**, *232*, 980–992. [[CrossRef](#)]
4. Shu, J.; Liu, R.; Liu, Z.; Chen, H.; Tao, C. Simultaneous removal of ammonia nitrogen and manganese from wastewater using nitrite by electrochemical method. *Environ. Technol.* **2017**, *38*, 370–376. [[CrossRef](#)]
5. Ma, Y.; Zheng, X.; Fang, Y.; Xu, K.; Zhao, M. Autotrophic denitrification in constructed wetlands: Achievements and challenges. *Bioresour. Technol.* **2020**, *318*, 123778. [[CrossRef](#)]
6. Shu, J.; Liu, R.; Liu, Z.; Du, J.; Tao, C. Manganese recovery and ammonia nitrogen removal from simulation wastewater by pulse electrolysis. *Sep. Purif. Technol.* **2016**, *168*, 107–113. [[CrossRef](#)]
7. Yu, C.; Mei, Y.; Xue, Y.; Wu, C.; Ye, H.; Li, J.; Du, D. A novel approach for recovery of manganese from on-site manganese-bearing wastewater. *J. Clean. Prod.* **2019**, *227*, 675–682. [[CrossRef](#)]

8. Yu, W.; Polgári, M.; Gyollai, I.; Fintor, K.; Huang, H.; Szabó, M.; Du, Y. Microbial metallogenesis of early carboniferous manganese deposit in central Guangxi, South China. *Ore Geol. Rev.* **2021**, *136*, 104251. [[CrossRef](#)]
9. Liu, K.; Fan, L.; Li, Y.; Zhou, Z.; Chen, C.; Chen, B.; Yu, F. Concentrations and health risks of heavy metals in soils and crops around the Pingle manganese (Mn) mine area in Guangxi Province, China. *Environ. Sci. Pollut. R.* **2018**, *25*, 30180–30190. [[CrossRef](#)]
10. Shu, J.; Lin, F.; Chen, M.; Li, B.; Wei, L.; Wang, J.; Luo, Z.; Wang, R. An innovative method to enhance manganese and ammonia nitrogen leaching from electrolytic manganese residue by surfactant and anode iron plate. *Hydrometallurgy* **2020**, *193*, 105311. [[CrossRef](#)]
11. Parde, D.; Patwa, A.; Shukla, A.; Vijay, R.; Killedar, D.J.; Kumar, R. A review of constructed wetland on type, treatment and technology of wastewater. *Environ. Technol. Innov.* **2021**, *21*, 101261. [[CrossRef](#)]
12. Nuamah, L.A.; Li, Y.; Pu, Y.; Nwankwegu, A.S.; Haikuo, Z.; Norgbey, E.; Banahene, P.; Bofah-Buoh, R. Constructed wetlands, status, progress, and challenges. The need for critical operational reassessment for a cleaner productive ecosystem. *J. Clean. Prod.* **2020**, *269*, 122340. [[CrossRef](#)]
13. Tao, W. Microbial removal and plant uptake of nitrogen in constructed wetlands: Mesocosm tests on influencing factors. *Environ. Sci. Pollut. R.* **2018**, *25*, 36425–36437. [[CrossRef](#)] [[PubMed](#)]
14. Yang, Y.; Zhao, Y.; Liu, R.; Morgan, D. Global development of various emerged substrates utilized in constructed wetlands. *Bioresour. Technol.* **2018**, *261*, 441–452. [[CrossRef](#)]
15. Wang, Y.; Cai, Z.; Sheng, S.; Pan, F.; Chen, F.; Fu, J. Comprehensive evaluation of substrate materials for contaminants removal in constructed wetlands. *Sci. Total Environ.* **2020**, *701*, 134736. [[CrossRef](#)]
16. Wang, D.; Lin, H.; Ma, Q.; Bai, Y.; Qu, J. Manganese oxides in Phragmites rhizosphere accelerates ammonia oxidation in constructed wetlands. *Water Res.* **2021**, *205*, 117688. [[CrossRef](#)]
17. Liu, H.; Hu, Z.; Zhang, Y.; Zhang, J.; Xie, H.; Liang, S. Microbial nitrogen removal of ammonia wastewater in poly (butylenesuccinate)-based constructed wetland: Effect of dissolved oxygen. *Appl. Microbiol. Biot.* **2018**, *102*, 9389–9398. [[CrossRef](#)]
18. Chen, P.; Culbreth, M.; Aschner, M. Exposure, epidemiology, and mechanism of the environmental toxicant manganese. *Environ. Sci. Pollut. R.* **2016**, *23*, 13802–13810. [[CrossRef](#)]
19. Wang, Y.N.; Tsang, Y.F.; Wang, H.; Sun, Y.; Song, Y.; Pan, X.; Luo, S. Effective stabilization of arsenic in contaminated soils with biogenic manganese oxide (BMO) materials. *Environ. Pollut.* **2020**, *258*, 113481. [[CrossRef](#)]
20. Zhang, L.; Wang, J.; Qiao, H.; Liu, F.; Fu, Z. Synthesis of manganese oxides for adsorptive removal of ammonia nitrogen from aqueous solutions. *J. Clean. Prod.* **2020**, *272*, 123055. [[CrossRef](#)]
21. Bai, Y.; Su, J.; Wen, Q.; Huang, T.; Chang, Q.; Ali, A. Characterization and mechanism of Mn(II)-based mixotrophic denitrifying bacterium (*Cupriavidus* sp. HY129) in remediation of nitrate (NO₃⁻-N) and manganese (Mn(II)) contaminated groundwater. *J. Hazard. Mater.* **2021**, *408*, 124414. [[CrossRef](#)] [[PubMed](#)]
22. Tang, W.; Gong, J.; Wu, L.; Li, Y.; Zhang, M.; Zeng, X. DGGE diversity of manganese mine samples and isolation of a *Lysinibacillus* sp. efficient in removal of high Mn (II) concentrations. *Chemosphere* **2016**, *165*, 277–283. [[CrossRef](#)] [[PubMed](#)]
23. Barrio-Parra, F.; Elío, J.; De Miguel, E.; García-González, J.E.; Izquierdo, M.; Álvarez, R. Environmental risk assessment of cobalt and manganese from industrial sources in an estuarine system. *Environ. Geochem. Health* **2018**, *40*, 737–748. [[CrossRef](#)]
24. Li, R.; Gao, L.; Wu, Q.; Liang, Z.; Hou, L.; Yang, Z.; Chen, J.; Jiang, T.; Zhu, A.; Li, M. Release characteristics and mechanisms of sediment phosphorus in contaminated and uncontaminated rivers: A case study in South China. *Environ. Pollut.* **2021**, *268*, 115749. [[CrossRef](#)]
25. Huang, Z.; Tang, Y.; Zhang, K.; Chen, Y.; Wang, Y.; Kong, L.; You, T.; Gu, Z. Environmental risk assessment of manganese and its associated heavy metals in a stream impacted by manganese mining in South China. *Hum. Ecol. Risk Assess.* **2016**, *22*, 1341–1358. [[CrossRef](#)]
26. Jones, M.R.; Luther, G.W.; Mucci, A.; Tebo, B.M. Concentrations of reactive Mn(III)-L and MnO₂ in estuarine and marine waters determined using spectrophotometry and the leuco base, leucoberberlin blue. *Talanta* **2019**, *200*, 91–99. [[CrossRef](#)]
27. Tessier, A.; Campbell, P.G.C.; Bisson, M. Sequential extraction procedure for the speciation of particulate trace metals. *Anal. Chem.* **1979**, *51*, 844–851. [[CrossRef](#)]
28. Nica, I.; Zaharia, C.; Suteu, D. Hydrogel Based on Tricarboxy-Cellulose and Poly (Vinyl Alcohol) Used as Biosorbent for Cobalt Ions Retention. *Polymers* **2021**, *13*, 1444. [[CrossRef](#)]
29. Van Veenhuyzen, B.; Tichapondwa, S.; Hörstmann, C.; Chirwa, E.; Brink, H.G. High capacity Pb (II) adsorption characteristics onto raw-and chemically activated waste activated sludge. *J. Hazard. Mater.* **2021**, *416*, 125943. [[CrossRef](#)]
30. Buyang, S.; Yi, Q.; Cui, H.; Wan, K.; Zhang, S. Distribution and adsorption of metals on different particle size fractions of sediments in a hydrodynamically disturbed canal. *Sci. Total Environ.* **2019**, *670*, 654–661. [[CrossRef](#)]
31. Vázquez-Ortega, A.; Fein, J.B. Thermodynamic modeling of Mn (II) adsorption onto manganese oxidizing bacteria. *Chem. Geol.* **2017**, *464*, 147–154. [[CrossRef](#)]
32. Piazza, A.; Ciancio Casalini, L.; Pacini, V.A.; Sanguinetti, G.; Ottado, J.; Gottig, N. Environmental bacteria involved in manganese (II) oxidation and removal from groundwater. *Front. Microbiol.* **2019**, *10*, 119. [[CrossRef](#)] [[PubMed](#)]
33. Abatal, M.; Olguin, M.T.; Anastopoulos, I.; Giannakoudakis, D.A.; Lima, E.C.; Vargas, J.; Aguilar, C. Comparison of Heavy Metals Removal from Aqueous Solution by *Moringa oleifera* Leaves and Seeds. *Coatings* **2021**, *11*, 508. [[CrossRef](#)]
34. Long, J.; Huang, X.; Fan, X.; Peng, Y.; Xia, J. Effective adsorption of nickel (II) with *Ulva lactuca* dried biomass: Isotherms, kinetics and mechanisms. *Water Sci. Technol.* **2018**, *78*, 156–164. [[CrossRef](#)] [[PubMed](#)]

35. Fawzy, M.; Nasr, M.; Adel, S.; Nagy, H.; Helmi, S. Environmental approach and artificial intelligence for Ni(II) and Cd(II) biosorption from aqueous solution using *Typha domingensis* biomass. *Ecol. Eng.* **2016**, *95*, 743–752. [[CrossRef](#)]
36. Serencam, H.; Ozdes, D.; Duran, C.; Tufekci, M. Biosorption properties of *Morus alba* L. for Cd (II) ions removal from aqueous solutions. *Environ. Monit. Assess.* **2013**, *185*, 6003–6011. [[CrossRef](#)]
37. Tavlieva, M.P.; Genieva, S.D.; Georgieva, V.G.; Vlaev, L.T. Thermodynamics and kinetics of the removal of manganese(II) ions from aqueous solutions by white rice husk ash. *J. Mol. Liq.* **2015**, *211*, 938–947. [[CrossRef](#)]
38. Xie, S.; Wen, Z.; Zhan, H.; Jin, M. An Experimental Study on the Adsorption and Desorption of Cu(II) in Silty Clay. *Geofluids* **2018**, *2018*, 3610921. [[CrossRef](#)]
39. Iftekhhar, S.; Ramasamy, D.L.; Srivastava, V.; Asif, M.B.; Sillanpää, M. Understanding the factors affecting the adsorption of Lanthanum using different adsorbents: A critical review. *Chemosphere* **2018**, *204*, 413–430. [[CrossRef](#)]
40. Ibrahim, H.A.; Doudoug, W.E.; Hefni, H.H.H.; El-Sawy, A.A.; Kamal, H.; Mahmoud, K. Removal of Ni (II), Mn (II) and Zn (II) from crude yellow cake aqueous solution by cross-linked chitosan and polyvinyl alcohol. *Egypt. J. Pet.* **2021**, *30*, 61–69. [[CrossRef](#)]
41. Nowruz, R.; Heydari, M.; Javanbakht, V. Synthesis of a chitosan/polyvinyl alcohol/activate carbon biocomposite for removal of hexavalent chromium from aqueous solution. *Int. J. Biol. Macromol.* **2020**, *147*, 209–216. [[CrossRef](#)] [[PubMed](#)]
42. Sareban, Z.; Javanbakht, V. Preparation and characterization of a novel nanocomposite of clinoptilolite/maghemite/chitosan/urea for manganese removal from aqueous solution. *Korean J. Chem. Eng.* **2017**, *34*, 2886–2900. [[CrossRef](#)]
43. Idrees, M.; Batool, S.; Ullah, H.; Hussain, Q.; Al-Wabel, M.I.; Ahmad, M.; Hussain, A.; Riaz, M.; Ok, Y.S.; Kong, J. Adsorption and thermodynamic mechanisms of manganese removal from aqueous media by biowaste-derived biochars. *J. Mol. Liq.* **2018**, *266*, 373–380. [[CrossRef](#)]
44. Campillo-Cora, C.; Conde-Cid, M.; Arias-Estévez, M.; Fernández-Calviño, D.; Alonso-Vega, F. Specific Adsorption of Heavy Metals in Soils: Individual and Competitive Experiments. *Agronomy* **2020**, *10*, 1113. [[CrossRef](#)]
45. Muliwa, A.M.; Onyango, M.S.; Maity, A.; Ochieng, A. Remediation of manganese in mine impacted water by clay/manganese oxide hybrid adsorbent: Equilibrium, kinetics and thermodynamic studies. *Int. J. Environ. Sci. Technol.* **2019**, *16*, 1985–1998. [[CrossRef](#)]
46. Rahman, M.S.; Clark, M.W.; Yee, L.H.; Burton, E.D. Arsenic(V) sorption kinetics in long-term arsenic pesticide contaminated soils. *Appl. Geochem.* **2019**, *111*, 104444. [[CrossRef](#)]
47. Largitte, L.; Pasquier, R. A review of the kinetics adsorption models and their application to the adsorption of lead by an activated carbon. *Chem. Eng. Res. Des.* **2016**, *109*, 495–504. [[CrossRef](#)]
48. Wang, C.; Boithias, L.; Ning, Z.; Han, Y.; Sauvage, S.; Sánchez-Pérez, J.; Kuramochi, K.; Hatano, R. Comparison of Langmuir and Freundlich adsorption equations within the SWAT-K model for assessing potassium environmental losses at basin scale. *Agric. Water Manag.* **2017**, *180*, 205–211. [[CrossRef](#)]
49. Elbana, T.A.; Magdi Selim, H.; Akrami, N.; Newman, A.; Shaheen, S.M.; Rinklebe, J. Freundlich sorption parameters for cadmium, copper, nickel, lead, and zinc for different soils: Influence of kinetics. *Geoderma* **2018**, *324*, 80–88. [[CrossRef](#)]
50. Hendrix, K.; Bleyen, N.; Mennecart, T.; Bruggeman, C.; Valcke, E. Sodium azide used as microbial inhibitor caused unwanted by-products in anaerobic geochemical studies. *Appl. Geochem.* **2019**, *107*, 120–130. [[CrossRef](#)]
51. Cabrol, L.; Quéméneur, M.; Misson, B. Inhibitory effects of sodium azide on microbial growth in experimental resuspension of marine sediment. *J. Microbiol. Meth.* **2017**, *133*, 62–65. [[CrossRef](#)] [[PubMed](#)]
52. Iram, S.; Shabbir, R.; Zafar, H.; Javaid, M. Biosorption and Bioaccumulation of Copper and Lead by Heavy Metal-Resistant Fungal Isolates. *Arab. J. Sci. Eng.* **2015**, *40*, 1867–1873. [[CrossRef](#)]
53. Nafiu, A.; Aliyu, A.A.; Aisha, A. Heavy metals and soil microbes. *Environ. Chem. Lett.* **2017**, *15*, 65–84. [[CrossRef](#)]